



## Urban flood modeling using deep-learning approaches in Seoul, South Korea

Xinxiang Lei<sup>a</sup>, Wei Chen<sup>a,b</sup>, Mahdi Panahi<sup>c,d</sup>, Fatemeh Falah<sup>e</sup>, Omid Rahmati<sup>f</sup>, Evelyn Uuemaa<sup>g</sup>, Zahra Kalantari<sup>h</sup>, Carla Sofia Santos Ferreira<sup>i</sup>, Fatemeh Rezaie<sup>d,j</sup>, John P. Tiefenbacher<sup>k</sup>, Saro Lee<sup>d,j,\*</sup>, Huiyuan Bian<sup>a</sup>

<sup>a</sup> College of Geology and Environment, Xi'an University of Science and Technology, Xi'an 710054, China

<sup>b</sup> Key Laboratory of Coal Resources Exploration and Comprehensive Utilization, Ministry of Natural Resources, Xi'an 710021, China

<sup>c</sup> Division of Science Education, College of Education # 4-301, Gangwondaehak-gil Chuncheon-si, Kangwon National University, Gangwon-do 24341, Republic of Korea

<sup>d</sup> Geoscience Platform Research Division, Korea Institute of Geoscience and Mineral Resources (KIGAM), 124, Gwahak-ro Yuseong-gu, Daejeon 34132, Republic of Korea

<sup>e</sup> Department of Watershed Management, Faculty of Natural Resources and Agriculture, Lorestan University, Lorestan, Iran

<sup>f</sup> Soil Conservation and Watershed Management Research Department, Kurdistan Agricultural and Natural Resources Research and Education Center, AREEO, Sanandaj, Iran

<sup>g</sup> Department of Geography, Institute of Ecology and Earth Sciences, University of Tartu, Vanemuise 46, 50410 Tartu, Estonia

<sup>h</sup> Department of Physical Geography and Bolin Centre for Climate Research, Stockholm University, Stockholm, Sweden

<sup>i</sup> Research Centre for Natural Resources, Environment and Society (CERNAS), Polytechnic Institute of Coimbra, Agrarian School of Coimbra, Coimbra, Portugal

<sup>j</sup> Department of Geophysical Exploration, Korea University of Science and Technology, 217 Gajeong-ro Yuseong-gu, Daejeon 34113, South Korea

<sup>k</sup> Department of Geography, Texas State University, San Marcos, TX 78666, United States

### ARTICLE INFO

#### Keywords:

Flood inundation  
Cities  
GIS  
Deep-learning  
Predictors

### ABSTRACT

Identification of flood-prone sites in urban environments is necessary, but there is insufficient hydraulic information and time series data on surface runoff. To date, several attempts have been made to apply deep-learning models for flood hazard mapping in urban areas. This study evaluated the capability of convolutional neural network (NNET<sub>C</sub>) and recurrent neural network (NNET<sub>R</sub>) models for flood hazard mapping. A flood-inundation inventory (including 295 flooded sites) was used as the response variable and 10 flood-affecting factors were considered as the predictor variables. Flooded sites were then spatially randomly split in a 70:30 ratio for building flood models and for validation purposes. The prediction quality of the models was validated using the area under the receiver operating characteristic curve (AUC) and root mean square error (RMSE). The validation results indicated that prediction performance of the NNET<sub>C</sub> model (AUC = 84%, RMSE = 0.163) was slightly better than that of the NNET<sub>R</sub> model (AUC = 82%, RMSE = 0.186). Both models indicated that terrain ruggedness index was the most important predictor, followed by slope and elevation. Although the model output had a relative error of up to 20% (based on AUC), this modeling approach could still be used as a reliable and rapid tool to generate a flood hazard map for urban areas, provided that a flood inundation inventory is available.

### 1. Introduction

In urban areas, floods typically cause significant loss of life and material damage due to the high density of residents and property (Karamouz et al., 2011; Cherqui et al., 2015; Zhao et al., 2020). Urban floods disrupt communication, power, and transportation systems, and thus essential supply chains (Anni et al., 2020). Between 2001 and 2018,

floods caused 66,078 deaths worldwide and affected 1.4 billion people. They also caused damages estimated at USD 309.4 billion (UN-Water, 2020). Urban areas are of particular concern, as the urban population is expected to increase from the current level of 55% of world's population to 60% by 2030 and 66% by 2050. Moreover, Asian cities are among the fastest-growing urban agglomerations in the world (UN-Water, 2020). In recent years, increases in the severity and frequency of urban flooding

\* Corresponding author at: Geoscience Platform Research Division, Korea Institute of Geoscience and Mineral Resources (KIGAM), 124, Gwahak-ro Yuseong-gu, Daejeon 34132, Republic of Korea.

E-mail address: [leesaro@kigam.re.kr](mailto:leesaro@kigam.re.kr) (S. Lee).

have been recorded. They are driven by extreme weather, rapid urbanization, and climate change (Anni et al., 2020). Floods in urban areas are generally triggered by intense rainfall, which is a major concern given the changes in rainfall patterns expected in response to future climate change (Easterling et al., 2000). Expansion of impervious surfaces (e.g., construction of buildings and roads) has major impacts on rainfall-runoff processes as they decrease infiltration and water-retention capacity (Kalantari et al., 2017; Ferreira et al., 2018). The ability of artificial drainage systems to rapidly transport runoff from urban areas is a critical parameter affecting the impacts of urban flooding. Table 1.

Accurate flood susceptibility mapping can provide meaningful information to support flood mitigation and management decisions. Although urban hydrology has been studied for decades, the complex interactions between hydrological, hydrometeorological, and land surface factors, and their roles in urban flooding, remain unclear (Nguyen and Bae, 2020). To manage floods effectively and prevent loss of human life and property, identification of flood-prone zones is urgently needed (Lee et al., 2017; Wang et al., 2019). Flood susceptibility mapping methods have improved over the years following advances in remote sensing, artificial intelligence, computational capacity, and geographic information systems. At present, such maps are largely based on flood inventories, bivariate and multivariate statistical relationships between hydrological datasets (Kalantari et al., 2019), and the results of physically based models (Zhang and Pan, 2014). However, these approaches require large amounts of data that are difficult to collect in urban areas. They also assume predefined relationships between controlling factors and flood occurrence that may not adequately describe the nonlinear dynamic characteristics of floods, which introduces uncertainty into the evaluation results (Rahmati et al., 2019). In recent years, machine learning has been coupled with geospatial analyses and applied in numerous studies related to flood vulnerability mapping. Machine learning uses computer algorithms to evaluate information and develop predictions by being trained with a specially developed dataset. This approach is particularly useful in data-scarce areas. Several machine-learning algorithms, including support vector machines (Rahmati et al., 2020), artificial neural networks (Michelsen et al., 2016; Falah et al., 2019) and random forest classification (Wang et al., 2019), have been successfully applied in flood-modeling studies. Such models predict susceptibility to flood hazards based on the statistical relationship between causal factors and inundation events, obtaining information directly from the data with only one assumption: future floods will occur under similar circumstances as past floods (Xu et al., 2018; Zhao et al., 2020). Machine-learning approaches achieve better results than other flood-susceptibility assessment methods, although their performance varies with the algorithm used (Wang et al., 2019). Several machine-

learning models have also been employed to enhance flood management strategies by accurately predicting streamflow (Shiri and Kisi, 2010; Shiri et al., 2012; Nourani et al., 2014; Karimi et al., 2018; Petty and Dhingra, 2018). The development of models capable of predicting watershed streamflow is a growing endeavor in flood-risk research, but this is beyond the scope of this study. The drawbacks of conventional models for analyzing big data have recently been overcome by using deep learning, which can automatically extract image features and represents an important advance. The deep-learning approach greatly minimizes the dimensions of parameters in neural networks during the training phase and this produces more reliable disaster-risk maps. One of the most popular deep-learning models is convolutional neural network (NNET<sub>C</sub>). It has been applied in flood-susceptibility assessment in agricultural (Wang et al., 2019) and urban (Zhao et al., 2020) watersheds in China. Recently, Panahi et al. (2021) identified the flood-prone areas of an agricultural watershed in Golestan Province, Iran, using NNET<sub>C</sub> and recurrent neural networks (NNET<sub>R</sub>). Since an urban watershed is dominated by pavement, streets, buildings, and parking areas, its hydrological function and structural characteristics are very different from those of agricultural, forested, and mountainous watersheds. On the other hand, urban environments usually lack hydrometric stations and hydrological information is limited. They are known to be data-scarce areas.

A barrier to using NNET<sub>C</sub> for urban flood-susceptibility modeling is that its efficiency in this area of application has not been fully investigated (Zhao et al., 2020). More importantly, the efficiency of NNET<sub>R</sub> has not yet been assessed. However, several remote sensing studies (e.g., Li et al., 2019; Peng et al., 2019) have sought to classify satellite images for identifying flood extent. In addition, the NNET<sub>C</sub> model has been applied for rainfall-runoff simulation in urban areas (Kimura et al., 2020; Guo et al., 2021). These two applications were also beyond the scope of this work.

The main goal of this study was to map flood susceptibility in Seoul, South Korea, where flooding is the most common natural disaster experience. Major floods have been recorded in recent years (Park et al., 2020). Previous studies in the region have mapped flood susceptibility using boosted-tree and random-forest models (Lee et al., 2017). In this study, a new methodological framework using a deep-learning approach was developed to improve urban flood-inundation mapping. The main hypothesis tested in this study was that deep-learning models can efficiently identify zones of flood inundation in an urban watershed. Key objectives of the work were to: evaluate the capability of the NNET<sub>C</sub> and NNET<sub>R</sub> models for mapping flood susceptibility in Seoul, compare their efficiency in terms of goodness-of-fit and predictive performance, and determine the importance of various causal drivers of urban flooding. The main novel feature and contribution of this study is that it demonstrates that the complicated conditions of urban flood inundation in the context of limited data can be overcome by modeling using NNET<sub>C</sub> and NNET<sub>R</sub>.

## 2. Study area

Seoul, the capital of South Korea, has an approximate area of 605 km<sup>2</sup> and 9.7 million residents, making it a densely populated city (Ha et al., 2009). This megacity is located at about 37.5°N and 127.0°E (Fig. 1). It is surrounded by mountains with heights ranging from 111 to 836 m (Eum, 2008). Since the early 2000 s, the South Korean government has sought to transform Seoul into competitive global megacity (Kim and Han, 2012). This highly developed city is now among the major cities in Asia (Hales et al., 2018). In recent years, its population has stabilized due to the high cost of housing and to a program to control city sprawl through the formation of satellite cities near Seoul (Lee et al., 2018). Annual precipitation in Seoul (1200–1600 mm) is higher than that in other areas at the same latitude due to its monsoon climate. Roughly 65% of annual rainfall occurs during the summer, which can lead to flooding (Kim et al., 2016). Due to topography and limited

**Table 1**  
Acronyms used in this study.

Acronym	Term
NNET <sub>C</sub>	Convolutional neural network
NNET <sub>R</sub>	Recurrent neural network
SLF	Slope length factor
TWI	Topographic wetness index
SPI	Stream power index
TPI	Topographic position index
TRI	Terrain ruggedness index
DEM	Digital elevation model
TN	True negatives
TP	True positives
FP	False positives
FN	False negatives
TPR	True positive rate
FPR	False positive rate
ROC	Receiver operating characteristic
AUC	Area under the ROC curve
RMSE	Root mean square error

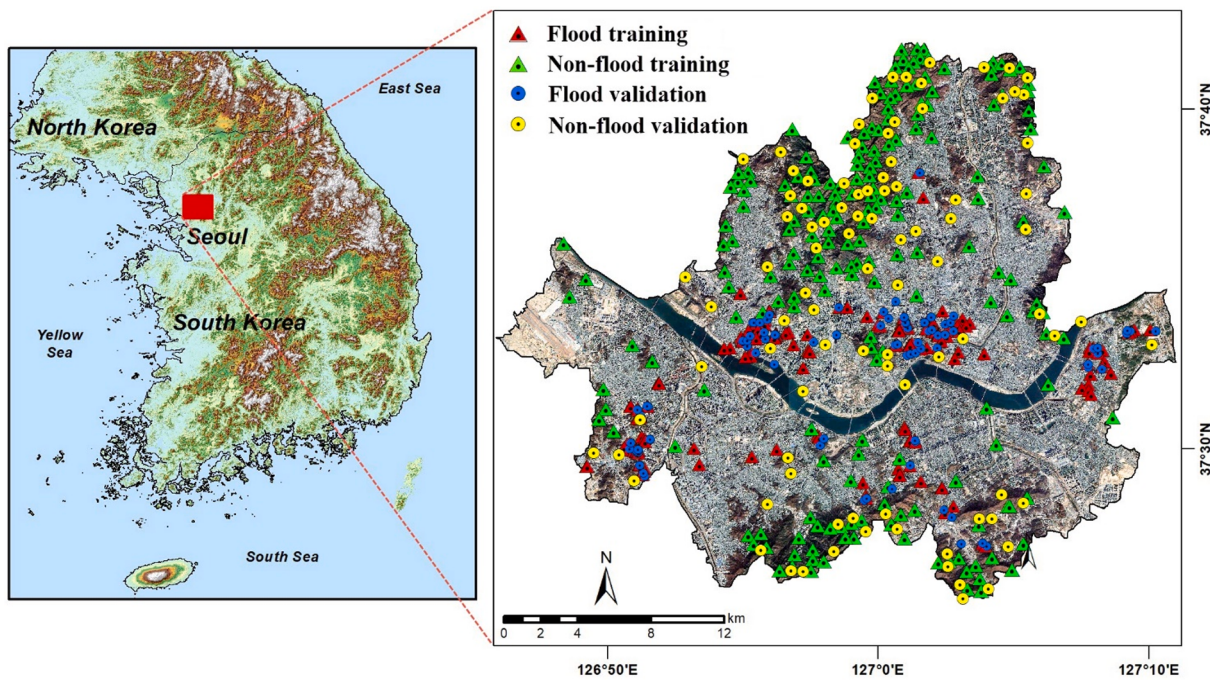


**Fig. 1.** Location of the study area in South Korea and map of flooded and non-flooded locations.

drainage capacity, lower-lying areas of Seoul have the highest flood risk (Shin and Park, 2014). Moreover, the existing retention and drainage infrastructure is inadequate for extreme precipitation events. Therefore, additional stormwater management procedures are needed (Kato and Endo, 2017).

### 3. Methodology

The methodological steps were as follows (Fig. 2):

- I. Database construction (section 3.1)
- II. Urban flood hazard mapping (section 3.2)
- III. Evaluation of model accuracy (section 3.3.)

### IV. Importance of variables (section 3.4)

#### 3.1. Database construction

##### 3.1.1. Flood inundation inventory

The locations of flood inundation from 2018 to 2020 were recorded using a GPS device. A flood inundation map was created that included 295 inundated locations. The flood inundation dataset was randomly split into two datasets for training (70% of data, n = 207) and validation (30% of data, n = 88) (Fig. 1). The training data were used to build and calibrate the model and the validation data were used to evaluate the accuracy of the model (Wang et al., 2019). Accuracies of modeling based

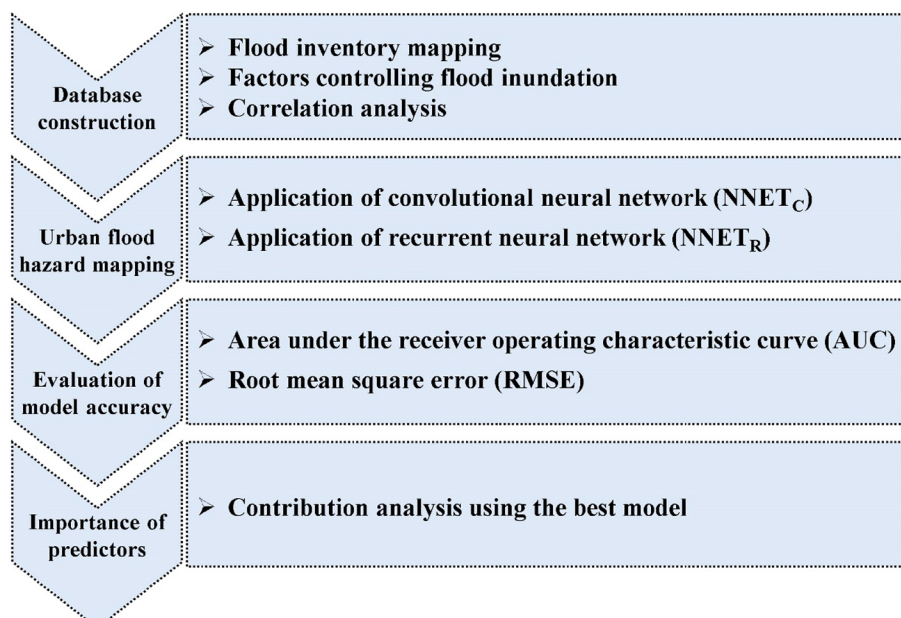


**Fig. 2.** Methodological flowchart of the study.

on training and validation data are referred to as goodness-of-fit and predictive skill, respectively. Spatial modeling with machine learning requires flood-present (1) and flood-absent (0) location data (Termeh et al., 2018; Darabi et al., 2019). Approximately equal numbers of flood-present and flood-absent locations is recommended for flood inundation mapping (Tehrany et al., 2014; Zhao et al., 2019).

### 3.1.2. Factors controlling flood inundation

To predict flood probability in this environment, we selected 10 predictor variables (also referred to as explanatory factors), based on field observations and a literature review (Fernández and Lutz, 2010; Rahmati et al., 2019; Zhao et al., 2019). These variables were: elevation, slope, slope length factor (SLF), topographic wetness index (TWI), curvature, stream power index (SPI), topographic position index (TPI), distance to the river, terrain ruggedness index (TRI), and land use. Rainfall was not included as a predictor variable because the study area

was small in area, and thus the spatial variation in rainfall was relatively low. Previous studies have similarly opted not to use rainfall distribution for urban flood-hazard assessment (Fernandez and Lutz, 2010; Gigović et al., 2017; Sepehri et al., 2019).

**3.1.2.1. Elevation.** Elevation can affect rainfall characteristics and the direction of runoff (Sanders, 2007). A digital elevation model (DEM) with 2-m spatial resolution was extracted from the topographical database. Elevation ranged from 5 to 807 m (Fig. 3a).

**3.1.2.2. Slope.** Slope is an important cause of inundation and it influences water flow direction. In this study, slope data were derived from the DEM using ArcGIS 10.2. Slope varied from 0 to 84%; it was highest in the northern part of the city, which includes Bukhansan National Park (Fig. 3b).

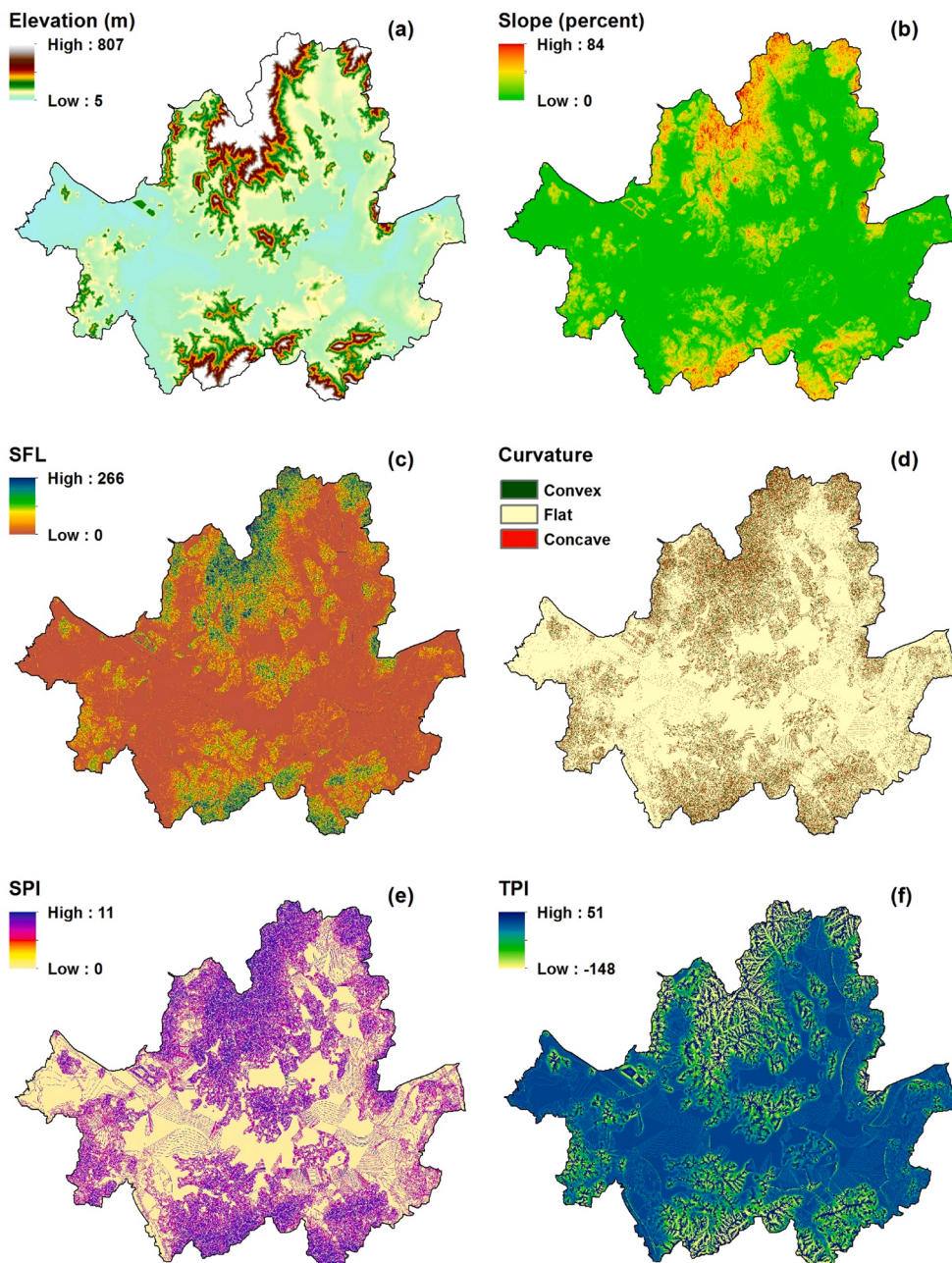


**Fig. 3.** Flood-influencing factors: a) elevation, b) slope percent, c) SLF, d) curvature, e) SPI, f) TPI, g) TRI, h) TWI, i) distance to river, and j) land use.

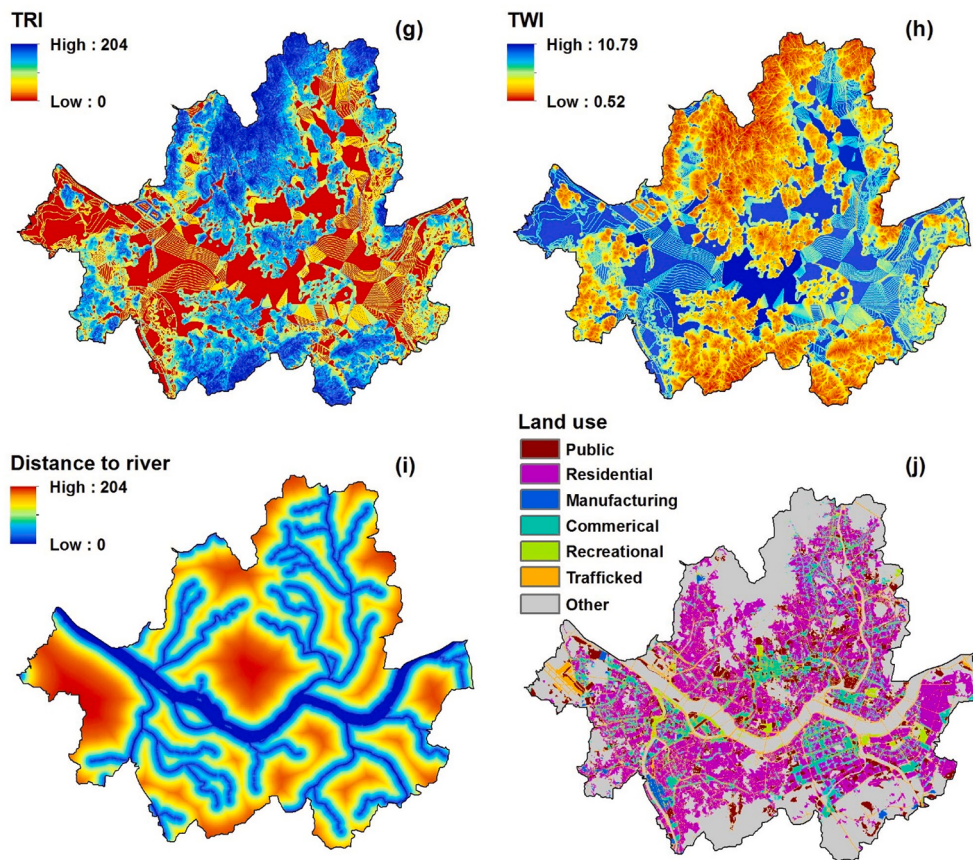


Fig. 3. (continued).

**3.1.2.3. Slope length factor (SLF).** SLF is one of the most important ways to describe the effects of topography and hydrology on soil erosion (Moore et al., 1991). It is a secondary factor calculated from the slope gradient and length (Rodríguez and Suárez, 2010). SLF was calculated using SAGA GIS software with the following equation (Moore et al., 1991):

$$SLF = (A_s/22.13)^{0.4} \times (\sin\beta/0.0896)^{1.3} \quad (1)$$

where  $A_s$  is the upstream contributing area ( $m^2$ ) and  $\beta$  is the slope in a given cell (degrees). SLF values in the study area ranged from 0 to 266 (Fig. 3c).

**3.1.2.4. Curvature.** Curvature is the morphometry of local topography and describes changes in slope inclination (Wilson and Gallant, 2000). Positive and negative values represent convex and concave areas, respectively, and values of zero indicate flat areas. Curvature influences the convergence or divergence of water during downslope flow. Concave curvature retains more water, thus increasing the risk of flooding (Rejith et al., 2019). A curvature map of the study area was produced using SAGA GIS software (Fig. 3d).

**3.1.2.5. Stream power index (SPI).** SPI, which estimates the erosive power of surface runoff, encompasses slope degree and catchment area (Burrough and McDonnell, 1998), both of which influence flood occurrence (Khosravi et al., 2018). SPI is a major factor controlling channel widening and thereby influences flooding (Righini et al., 2017). SPI was calculated using the following equation:

$$SPI = A_s \tan\beta \quad (2)$$

where  $A_s$  is the upstream contributing area ( $m^2$ ) and  $\beta$  is the slope in a given cell (degrees). SPI values in the study area ranged from 0 to 11

(Fig. 3e).

**3.1.2.6. Topographic position index (TPI).** TPI indicates the difference between the elevation of a focal cell and the mean elevation of neighboring cells. TPI was calculated using the following equation (Eq. (3)) (Guisan et al., 1999; Mokarrama and Hojati, 2018; Popa et al., 2019):

$$TPI = Z_0 - \sum_{1-n} Z_n/n \quad (3)$$

where  $Z_n$  is the elevation of cells (m) within the local window,  $Z_0$  is the elevation of the cell under evaluation (m), and  $n$  is the total number of neighboring cells employed in the evaluation. Since a  $3 \times 3$  filter was used,  $n$  was eight in this study. The TPI value in the study area varied from -148 to 51 (Fig. 3f). Positive values of TPI indicate that the focal cell is higher than adjacent areas, while negative values denote a focal cell that is lower than adjacent areas, as generally occurs in valleys (De Reu et al., 2013). Zero values of TPI indicate flat areas (Weiss, 2001).

**3.1.2.7. Terrain ruggedness index (TRI).** TRI is useful for flood-inundation modeling (Riley et al., 1999). Flat areas have a value of zero, whereas strong positive TRI values are found in mountain areas with steep ridges. TPI represents the roughness of the surface, which along with the objects on it (e.g., vegetation, buildings) creates hydrodynamic friction (Dorn et al., 2014). A TRI map was produced using SAGA-GIS. TRI values in the study area ranged from 0 to 204 (Fig. 3g).

**3.1.2.8. Topographic wetness index (TWI).** TWI is used to estimate hydrological responses to topographic characteristics (Beven and Kirkby, 1979; Mokarrama and Hojati, 2018) or to map spatial patterns of soil moisture (Radula et al., 2018). TWI is a function of the upstream contributing area ( $a$ ) and slope degree ( $\tan\theta$ ):

$$\text{TWI} = \ln\alpha/\tan\theta \quad (4)$$

In the study area, TWI ranged from 0.52 to 10.79 (Fig. 3h), with higher values indicating wetter areas.

**3.1.2.9. Distance to the river.** Riverbanks and flood plains are at the highest risk of inundation, so distance to the nearest river is important when modeling floods (Predick and Turner, 2008; Mignot et al., 2019). Euclidean distances to the Han River system were calculated as continuous values from 0 to 204 m in the study area (Fig. 3j). Distance to the river was generated using the flow direction and Euclidian distance functions in ArcGIS 10.2.

**3.1.2.10. Land use.** Runoff conditions vary considerably among different land use and land cover patterns (Darabi et al., 2019). Built-up areas generate more surface runoff than vegetated areas (Tehrany et al., 2015a). Therefore, land use is a key factor in flood risk (Beckers et al., 2013). We identified seven land use classes in the study area: public, residential, manufacturing, commercial, recreational, traffic, and other (Fig. 3k).

More information is provided (Table 2). All of the input layers (predictor variables) were standardized before being used in the models.

### 3.1.3. Correlation analysis

Although predictor variables were selected from a review of the literature review, the spatial autocorrelation of these variables was a concern. Autocorrelated predictors can lead to significant overfitting (Meyer et al., 2019). In this study, Pearson's correlation test was run using the Band Collection Statistics tool in ArcGIS 10.2 (Table 3). The analysis revealed that there were no statistically significant correlations between predictor variables ( $p > 0.05$ ).

## 3.2. Urban flood hazard mapping

### 3.2.1. Application of convolutional neural network (NNET<sub>C</sub>) models

The NNET<sub>C</sub> model uses deep learning and has shown promise for image classification and recognition (Hu et al., 2015). The basic architecture of a NNET<sub>C</sub> comprises a feature-extraction layer (containing a pooling layer and a convolutional layer) and a feature-mapping layer (or fully connected layer). The convolutional layer consists of convolution units, parameters optimized using a back-propagation algorithm (Kang et al., 2019). The convolution step considers the features of predictive variables and determines their weights. The input and output for each stage in the model architecture are sets of arrays referred to as feature maps. For example, if the input is a two-dimensional image  $x$ , the input is first decomposed into a sequential array of  $x = \{x_1, x_2, \dots, x_N\}$ . The convolutional layer is defined as:

$$y_i = f \left( b_j + \sum_i k_{ij} * x_i \right) \quad (5)$$

where  $y_j$  is the  $j^{th}$  output for the convolutional layer,  $x_i$  refers to each input feature map,  $k_{ij}$  represents the convolutional kernel with the  $i^{th}$  predictive variable designated  $x_i$ ,  $b_j$  is a trainable bias, and  $f$  denotes the nonlinear function.

The size of the feature map output from the convolutional layer is reduced by the pooling layer through down-sampling. This process can ultimately improve the overfitting problem with the model, while sharply reducing the computation cost in the absence of changes to the structure of the image. When the amount of input data is very large, the pooling layer retains the most crucial information and reduces the number of parameters. There are various types of pooling layers (e.g., max, average, sum, and so forth). Max pooling, a frequent subsampling layer, reduces the size of the convolutional layer output by computing the maximum value for each patch of the feature map, leading to considerable improvement in detection of important features (Gopalakrishnan et al., 2017). In fact, the output of the max pooling layer contains the key information from the previous stage (Kumar and Hati, 2020).

The last layer in the NNET<sub>C</sub> architecture, the fully connected layer, contains neurons which integrate the features obtained from multiple feature maps extracted by the convolutional layer. Using a softmax activation function, the output vector is mapped to values between 0 and 1 that indicate the predicted probability of this category (Kang et al., 2019).

### 3.2.2. Application of recurrent neural network (NNET<sub>R</sub>) models

NNET<sub>R</sub> models are artificial neural networks with recurrent connections that analyze large datasets to make predictions (Bengio et al., 1994). These models have a memory of past results, which is beneficial for predicting time-dependent objectives. NNET<sub>R</sub> models are well suited to supervised learning problems where the dataset has a sequential nature. The aim of supervised learning is to predict future results from past data. A training set containing a given target (an output) and several input variables can be used to predict target values. The final outputs of an artificial neural network can be continuous (regression) or categorical (classification) (Petneházi, 2019).

NNET<sub>R</sub> models use high-dimensionality hidden states with nonlinear dynamics (Sutskever et al., 2011). They can be used to extract dynamic behaviors from complex systems based on internal recurrence and can be trained to understand time-varying or sequential patterns (Chang et al., 2014). NNET<sub>R</sub> models have been used to forecast hydrological processes (e.g., water level prediction) as they are able to learn and model nonlinear relationships (Ren et al., 2020). Hidden states act as the memory of the network, and the state of the hidden layer at any given time is dependent on its previous state (Mikolov et al., 2006). Input, recurrent hidden, and output layers comprise the NNET<sub>R</sub>. The input layer has  $N$  input units, and the inputs are a sequence of vectors through time  $t \{ \dots, x_{t-1}, x_t, x_{t+1}, \dots \}$ . The input data are connected to the hidden layer. The hidden layer has  $M$  hidden units  $h_t = (h_1, h_2, \dots, h_M)$ , which are connected to each other through time with recurrent connections (Sutskever et al., 2013). The hidden layer defines the state space or "memory" of the system as:

$$h_t = fH(0_t) \quad (6)$$

$$0_t = W_{IH}X_t + W_{HH}h_{t-1} + b_h \quad (7)$$

where  $fH(\cdot)$  defines the hidden layer activation function and  $b_h$  refers to the bias vector of the hidden units. The hidden units and output layer are connected through weighted connections (called  $W_{HO}$ ). The output layer has  $P$  units  $y_t = (y_1, y_2, \dots, y_P)$ , which are calculated:

$$y_t = fo(W_{HO}h_t + b_0) \quad (8)$$

**Table 2**  
Information on the flood influential factors.

Factors	Scale	Source	Format
Elevation	1:25000	ALOS PALSAR DEM	Grid
Slope	1:25000	ALOS PALSAR DEM	Grid
Slope length factor (SLF)	1:25000	ALOS PALSAR DEM	Grid
Topographic wetness index (TWI)	1:25000	ALOS PALSAR DEM	Grid
Plan curvature	1:25000	ALOS PALSAR DEM	Grid
Stream power index (SPI)	1:25000	ALOS PALSAR DEM	Grid
Topographic position index (TPI)	1:25000	ALOS PALSAR DEM	Grid
Distance to the river	1:5000	National Geographic Information Institute	Grid
Terrain ruggedness index (TRI)	1:25000	ALOS PALSAR DEM	Grid
Land use	1:5000	Ministry of Environment	Polygon

**Table 3**

Pairwise correlation matrix of flood influential factors in the study area.

Factor	Elevation	Slope	SLF	Plan curvature	SPI	TPI	TRI	TWI	Distance to river	Land use
Elevation	1.00	0.33	0.31	0.25	0.05	0.37	0.34	0.36	-0.05	0.36
Slope	0.33	1.00	0.44	-0.05	0.06	0.32	0.64	0.53	-0.05	0.17
SLF	0.31	0.44	1.00	0.21	0.53	0.33	0.46	0.38	-0.07	0.19
Plan curvature	0.25	-0.05	0.21	1.00	0.04	0.22	0.06	0.04	-0.13	0.20
SPI	0.05	0.06	0.53	0.04	1.00	0.06	0.12	0.05	0.01	0.02
TPI	0.37	0.32	0.33	0.22	0.06	1.00	0.34	0.31	-0.10	0.22
TRI	0.34	0.64	0.46	0.06	0.12	0.34	1.00	0.61	-0.05	0.18
TWI	0.36	0.53	0.38	0.04	0.05	0.31	0.61	1.00	-0.03	0.15
Distance to river	-0.05	-0.05	-0.07	-0.13	0.01	-0.10	-0.05	-0.03	1.00	0.01
Land use	0.36	0.17	0.19	0.20	0.02	0.22	0.18	0.15	0.01	1.00

where  $f_0(\cdot)$  refers to the activation function and  $b_0$  defines the bias vector in the output layer (Sutskever et al., 2011).

### 3.3. Evaluation of model accuracy

The growing availability of numerous learning algorithms with differing success rates has made the task of appropriate model selection crucially important and highlights the need for evaluation criteria (Wu and Flach, 2005). The receiver operating characteristic (ROC) curve is a popular technique for accuracy evaluation of binary classification models (Gajowniczek et al., 2014).

The ROC curve is a confusion matrix with four categories of data: true negatives (TN, data correctly regarded as negative), true positives (TP, data correctly regarded as positive), false negatives (FN, data incorrectly regarded as negative), and false positives (FP, data incorrectly regarded as positive) (Davis and Goadrich, 2006). Model performance metrics such as the true positive rate (TPR; the proportion of instances labeled positive that were correctly predicted), which is plotted on the y-axis, and false positive rate (FPR; the proportion of instances labeled positive that were incorrectly labeled as negative), which is plotted on x-axis, are derived from the confusion matrix. The upper left-hand corner of the ROC curve, where FPR is 0 and TPR is 1, is the optimal point on the ROC curve. Eqs. (9) and (10) define the area under the ROC curve (AUC):

$$X = 1 - \text{specificity} = 1 - \frac{TN}{FP + TN} \quad (9)$$

$$Y = \text{sensitivity} = \frac{TP}{TP + FN} \quad (10)$$

AUC was used to determine the accuracy of the models tested in this study. Yesilnacar (2005) classified the relationship between the AUC value and the predictive skill of models as poor, average, good, very good, and excellent, using the categories 0.5–0.6, 0.6–0.7, 0.7–0.8, 0.8–0.9, and 0.9–1.0, respectively.

Root mean square error (RMSE) was calculated as a complementary metric using the equation:

$$RMSE = \sqrt{\frac{\sum_{i=1}^N (f_i - \bar{f}_i)^2}{N}} \quad (11)$$

where  $f$  is the estimated flood susceptibility,  $\bar{f}$  is the observed flood susceptibility, and  $N$  is the total number of flooded sites. Like the AUC metric, RMSE was calculated for each model in both the training and validation steps.

### 3.4. Importance of variables

Machine-learning models allow the importance of predictor variables to be estimated based on contribution analysis (Williamson et al., 2021). The importance of variables was investigated using the method proposed by Xia et al. (2021) which focuses on the values of the global

max pooling layer and weights in the output layer. The importance of variables was determined for both models.

## 4. Results

### 4.1. Urban flood susceptibility mapping

The aim of this study was to map flood-prone areas in Seoul utilizing the NNET<sub>C</sub> and NNET<sub>R</sub> approaches. To achieve this goal, thematic layers of 10 flood-related factors (elevation, slope, SLF, curvature, SPI, TPI, TRI, TWI, distance to the river, and land use) were overlaid with 70% of the flooded points that comprised the training set. The flood risk maps were categorized areas into five classes by flood potential (very high, high, moderate, low, or very low), which covered, respectively, 20.24%, 21.05%, 19.2%, 19.63%, and 19.88% of the NNET<sub>C</sub> map and 20.6%, 19.59%, 20.21%, 19.72%, and 19.88% of the NNET<sub>R</sub> model results (Fig. 4). These maps show that nearly 40% of the study area is likely to be affected by flooding. Visually, it is apparent that the flood points (in both the testing and training groups) agreed with the predicted flood maps.

### 4.2. Accuracy assessment

Based on AUC values, the accuracies of the models produced in the training and validation steps were very good (Fig. 5). In the training step, AUC values of 86% and 84% were obtained for the NNET<sub>C</sub> and NNET<sub>R</sub> models, respectively (Fig. 5a). It can be concluded that there was good agreement between flood locations (training group) and environmental factors. However, training flood locations were used in construction of the model, so the accuracy of the training phase does not represent the performance of the model. Therefore, validation data were used for the final assessment. For this purpose, the NNET<sub>C</sub> and NNET<sub>R</sub> flood maps generated were overlaid with 30% of the flood locations initially set aside for validation. The AUC values were 84% (NNET<sub>C</sub>) and 82% (NNET<sub>R</sub>) for the validation step (Fig. 5b), demonstrating strong performance of both models in predicting flood hazard probability.

The RMSE values confirmed the goodness-of-fit and predictive performance of the models (Fig. 6). In the training step, the NNET<sub>C</sub> and NNET<sub>R</sub> models had RMSE values of 0.147 and 0.158, respectively (Fig. 6e, 6g). These results indicate excellent goodness-of-fit between the training dataset and predictor variables. In the validation analysis (Fig. 6l, 6k), NNET<sub>C</sub> (RMSE = 0.163) showed better predictive performance than the NNET<sub>R</sub> model (RMSE = 0.186). Overall, both evaluation metrics indicated good agreement and in comparison NNET<sub>C</sub> was the better model.

### 4.3. Variable importance

According to the NNET<sub>C</sub> model, TRI is the most important factor in flood inundation in Seoul, with a contribution value of 16.17% in modeling (Fig. 7). It was followed by slope (15.5%), elevation (13.4%), and TWI (12.92%) (Fig. 7a). Land use (9.22%), SLF (9.84%), TPI

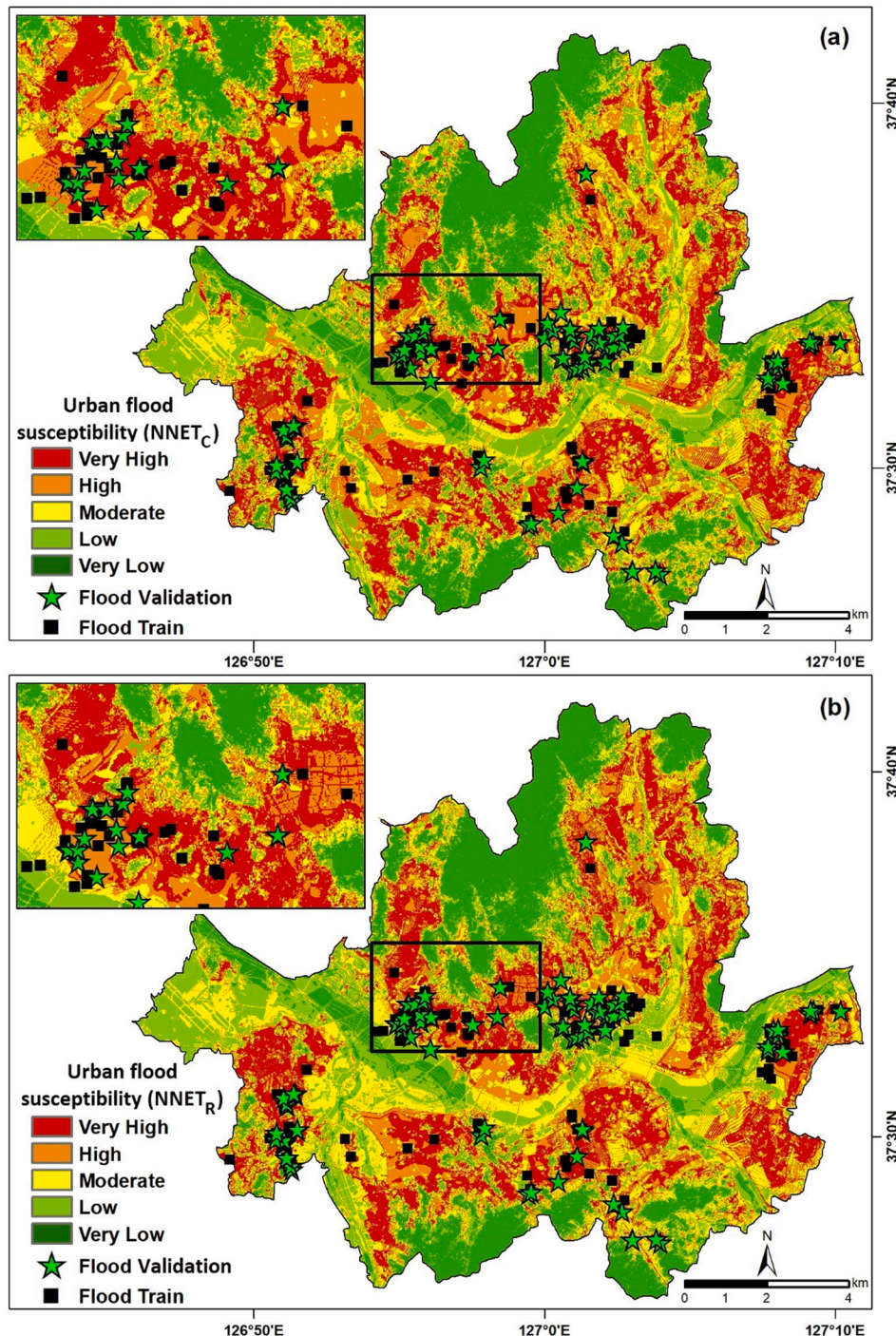


Fig. 4. Urban flood susceptibility maps produced using: a)  $NNET_C$  and b)  $NNET_R$ .

(7.93%), and plan curvature (6.72%) made medium contributions in flood inundation modeling using  $NNET_C$ . The lowest contributions were made by SPI (4.76%) and distance to river (3.9%). Results for the  $NNET_R$  model were similar in terms of relative importance (Fig. 7b). According to  $NNET_R$ , TRI (14.87%), slope (13.59%), and elevation (11.7%) were the most important predictor variables in urban flood hazard mapping of the study area. TWI, land use, SFL, TPI, and plan curvature made moderate contributions to the modeling. Like the  $NNET_C$  model, SPI (6.66%) and distance to river (6.21%) made the lowest contributions to urban flood modeling with the  $NNET_R$  model.

## 5. Discussion

### 5.1. Urban flood susceptibility maps

Flooding causes significant fatalities and properties globally. It is probably the most devastating and widespread natural disaster affecting humanity (Teng et al., 2017). Urban areas have higher flood risk due to the large proportion of rainfall that becomes runoff (Sato, 2006; Mignot et al., 2019). Moreover, urban growth has continuously encroached into spaces that rivers use for excess flows (Tockner et al., 2010). The quality of life in urban areas is dependent on the availability of services, and on energy and water provisioning, accommodation, education, and

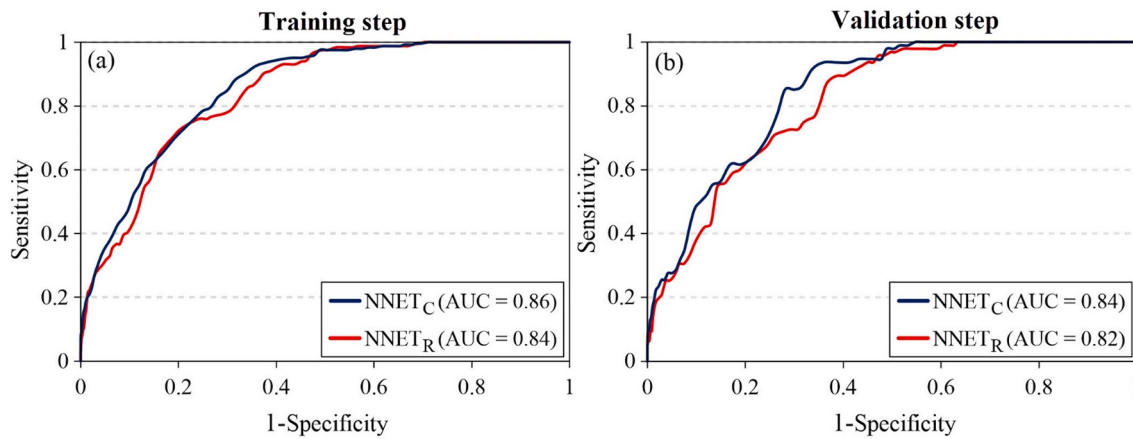


**Fig. 5.** Receiver operating characteristic (ROC) curves of the  $\text{NNET}_C$  and  $\text{NNET}_R$  models in the (a) training and (b) validation steps.

employment. Urban flooding causes significant disruption of such services, and thus has a major secondary impact on urban residents (Hammond et al., 2015). As it is impossible to prevent the occurrence of these extreme events, application of flood management strategies is crucial. Through precise analysis of previously flooded locations, flood-prone areas can be identified, and damages can be reduced through mitigative measures. Flood-susceptibility mapping is a widely used strategy for managing future floods (Kourgialas and Karatzas, 2011). Urban flood-vulnerability maps are also useful tools for planning urban land uses. Additionally, such maps can help engineers identify the areas that are most in need of discharge infrastructure (Büchele et al., 2006).

Flood inundation due to extreme rainfall events has been documented throughout Seoul's history. This megacity has a high concentration of political, economic, and other urban activities. Combined with high population density and complex buildings and underground networks, there is a high potential for considerable economic losses in future floods. In this study, two deep-learning models ( $\text{NNET}_C$ ,  $\text{NNET}_R$ ) were used to generate flood-susceptibility maps of Seoul to support land use planning and flood risk mitigation efforts. Based on the susceptibility maps generated, most of the study area possess high flood risk. Therefore, Seoul should receive the attention of scientists and government authorities to improve planning and mitigate flood risk to protect human life, property, and the immense infrastructure of this city. Otherwise, even small floods will continue to pose the prospects for major disasters.

## 5.2. Flood influencing factors

The results of this study indicate that TRI, slope, elevation, and TWI are the most important predictors of urban flooding in Seoul. They are followed by land use, SFL, TPI, plan curvature, SPI, and proximity to the river. Strong and significant relationships between flood occurrence and certain environmental variables are revealed by the final flood-susceptibility maps. Floods are more likely to occur in areas characterized by lower TRI, lower slope, lower elevation, and higher TWI values. High TWI values are strongly correlated with floodplain development (Naito and Cairns, 2011; Hong et al., 2018). Our findings are supported by previous studies conducted in the area, even though different predictor variables were used in this study (Lee et al., 2018). Higher slopes increase flow velocity, but flooding is unlikely to occur on steep slopes (Li et al., 2012). Instead, steep slopes cause flooding downstream and increase the destructive power of floods (Eini et al., 2020). Flat areas have little resistance to flow, making them more prone to flooding, especially in coastal areas. Flooding in Seoul is predicted to occur in areas of moderate slope and low elevation. Higher TWI occurs in large areas with low slopes, places that are more likely to flood. Lee et al. (2017) created flood-susceptibility maps of Seoul using boosted-tree and

random-forest models and showed that flooding is more likely in areas of lower elevation. Similar observations have been made worldwide. As discussed by Li et al. (2012), low-lying areas are highly prone to flooding and such areas also tend to have high population density, which increases exposure of people to floods. Slope length influences the time required for a molecule of water to flow from the top of a catchment to its outlet, and therefore influences flood risk (Rodríguez and Suárez, 2010). Tehrany et al. (2015b) similarly concluded that floods are more likely to occur in areas with low slopes and concave curvature, and that floods primarily occur at low elevations nearer riverbanks.

## 5.3. Comparison of model performance

The capabilities of the  $\text{NNET}_C$  model for modeling urban floods had not been investigated extensively (Zhao et al., 2020). More importantly, never had the  $\text{NNET}_R$  model been applied to mapping flood susceptibility. Our results indicate that both the  $\text{NNET}_C$  and  $\text{NNET}_R$  models performed very well ("very good" based on the accuracy classification in Yesilnacar (2005)). There was a slight difference in the accuracies of the models, but the  $\text{NNET}_C$  model was revealed to be more accurate in both the training and validation steps. Regarding model efficiency, previous research had shown that the random forest and support vector machine models were the benchmarks for flood susceptibility mapping (Tehrany et al., 2015b; Lee et al., 2017). Based on our results, we can strongly recommend the  $\text{NNET}_C$  and  $\text{NNET}_R$  models for accurate visualization of flood occurrence to enable risk mitigation and planning to protect life and property. The validation analysis supports the hypothesis that deep-learning models can efficiently determine the distribution of flood inundation in an urban watershed and that both  $\text{NNET}_C$  and  $\text{NNET}_R$  are suitable for flood-inundation analysis in urban settings. The  $\text{NNET}_C$  model, as explained by Hussain et al. (2020), has the benefit of reducing the number of parameters required for the convolutional layer by sharing the same convolution kernel among all spatial locations. This organization of convolution kernels promotes accurate learning (Wu, 2020). Previous studies have shown that  $\text{NNET}_C$  models can learn invariant representations and can achieve human-level performance with adequate training data, and that these models can acquire representations from grid-like data (Khan et al., 2020). The  $\text{NNET}_C$  model as a state-of-the-art machine-learning approach has performed excellently in relating to pattern recognition and computer vision (Wu, 2020).  $\text{NNET}_R$  models have also achieved breakthroughs in numerous sequence- and series-based learning tasks, and in language processing, image captioning, and speech recognition (Socher et al., 2011; Graves et al., 2013; Mao et al., 2014).  $\text{NNET}_R$  is known to perform well in learning tasks based on successive input data, and the  $\text{NNET}_R$  architecture is capable of modeling time-series data wherein each time-step depends on those that preceded it. Furthermore,  $\text{NNET}_R$  can handle variable-length

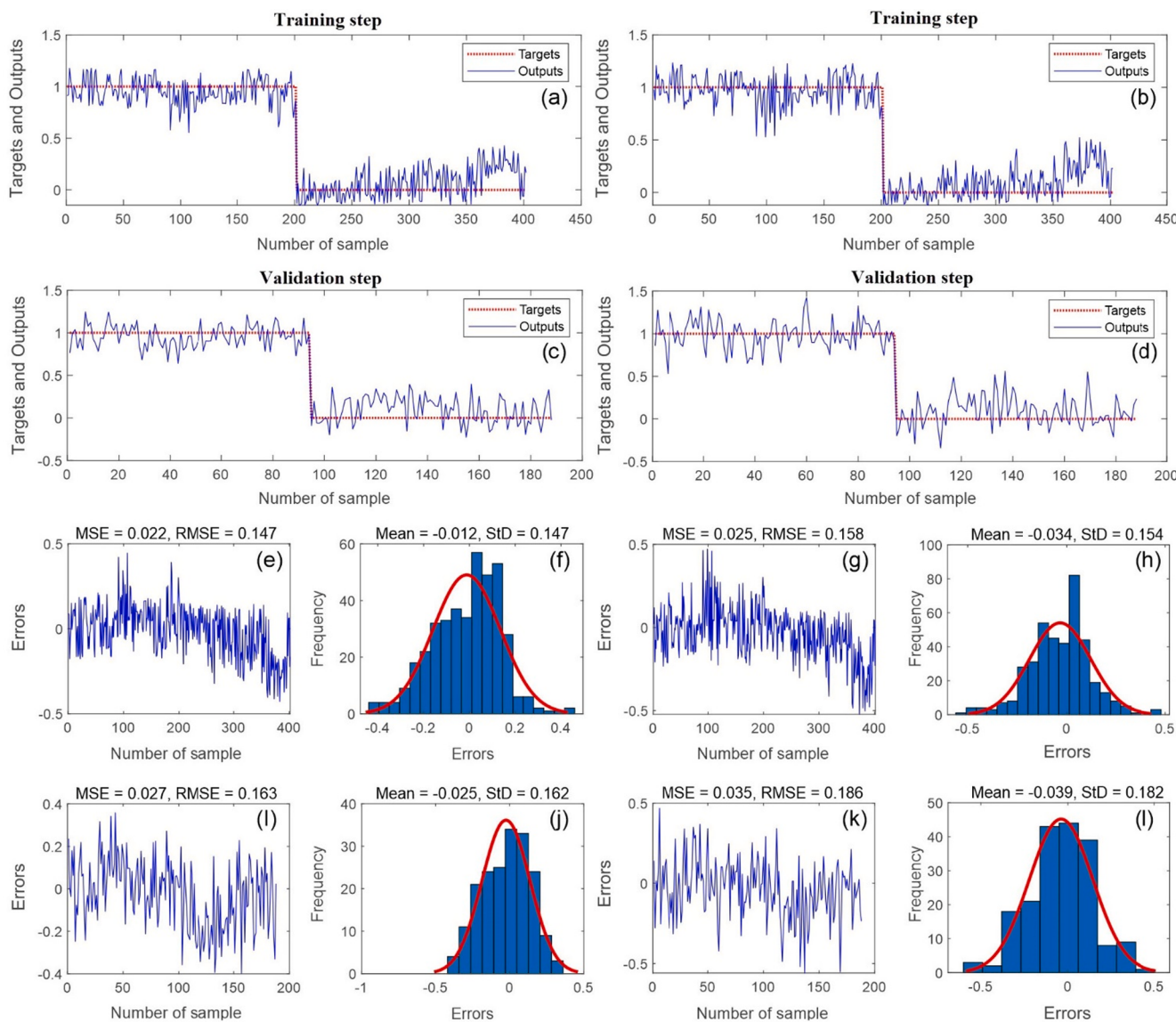


**Fig. 6.** Goodness-of-fit and predictive performances based on statistical metrics: a) target and output  $\text{NNET}_C$  value of train data samples; b) target and output  $\text{NNET}_R$  value of training data samples; c) target and output  $\text{NNET}_C$  value of testing data samples; d) target and output  $\text{NNET}_R$  value of testing data samples; e) MSE and RMSE value of the  $\text{NNET}_C$  model in the training phase; f) frequency errors of the  $\text{NNET}_C$  model using the training data samples; g) MSE and RMSE value of the  $\text{NNET}_R$  model in the training phase; h) frequency errors of the  $\text{NNET}_R$  model using the training data samples; i) MSE and RMSE value of the  $\text{NNET}_C$  model in the validation phase; j) frequency errors of the  $\text{NNET}_C$  model using the testing data samples; k) MSE and RMSE value of the  $\text{NNET}_R$  model in the validation phase; and l) frequency errors of the  $\text{NNET}_R$  model using the testing data samples.

inputs, eliminating the need for “padding inputs.” In contrast, the multilayer perceptron and  $\text{NNET}_C$  approaches are constrained by the sizes of inputs and outputs and the numbers of layers and computational steps.

Factors affecting the precision of a model can be investigated using the embedded functions of machine learning which identify underlying correlations in a dataset and make decisions without explicit instructions, thereby obtaining results with very low uncertainty (Khan et al., 2020). Moreover, machine learning allows model systems to learn from past data, recognize patterns, and make predictions for urban systems with minimal human interaction. This method can provide computers with the ability to learn and make decisions without explicit programming. Using such methods, computers can change programs when exposed to new data. Although some research has shown that the accuracy of machine-learning models can fluctuate with respect to different training-validation datasets (Xu and Mannor, 2012; Jalal Shiri et al., 2020; Naser Shiri et al., 2020), it was beyond the scope of this

study to scrutinize the effects of different training and validation data on the robustness of the models.

## 6. Conclusions

Flooding in Seoul is increasing. Most recent floods have affected roads in the inner city or in residential areas and have caused deaths and damage to property. Therefore, flood-susceptibility assessment is crucial for predicting the future disasters. This study applied  $\text{NNET}_C$  and  $\text{NNET}_R$  models to identify areas of high flood risk within Seoul, South Korea. The following conclusions were drawn:

- The validation tests demonstrated that the  $\text{NNET}_C$  model ( $AUC = 84\%$ ,  $RMSE = 0.163$ ) outperformed the  $\text{NNET}_R$  model ( $AUC = 82\%$ ,  $RMSE = 0.186$ ). Therefore, the  $\text{NNET}_C$  model can be used to map flood susceptibility in urban areas where hydraulic-based models are not appropriate due to data scarcity. However, the efficiency of both

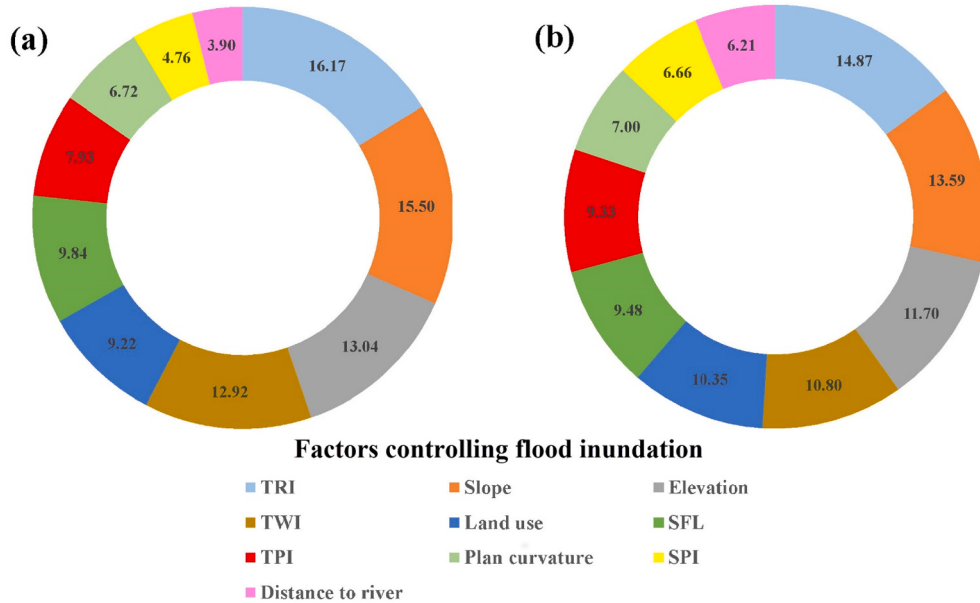


**Fig. 7.** Influences of predictive variables on urban flooding based on: a) NNET<sub>C</sub> and b) NNET<sub>R</sub> (values are in percentages).

models is very good, and both are robust and can be used for urban flood management. Therefore, application of both is highly recommended in future research, as they provide rapid, low-cost results.

- TRI was identified as the most important factor affecting urban flood risk in Seoul. Slope, elevation, TWI, land use, SFL, and TPI were secondarily important influencing factors. These factors should be analyzed by before construction of new infrastructure and housing projects. Other factors (curvature, SPI, distance to river) made weak or moderate contributions to the models.
- Both models successfully predicted flood-prone areas in Seoul, but further research is needed to determine the efficiency of their use in other urban areas. More work is needed to determine the effects of different training and testing datasets.

#### CRediT authorship contribution statement

**Xinxiang Lei:** Writing - original draft. **Wei Chen:** Writing - original draft. **Mahdi Panahi:** Conceptualization, Data curation, Methodology. **Fatemeh Falah:** Writing - original draft. **Omid Rahmati:** Conceptualization, Methodology, Writing - review & editing. **Evelyn Uuemaa:** Writing - review & editing. **Zahra Kalantari:** Writing - review & editing. **Carla Sofia Santos Ferreira:** Writing - review & editing. **Fatemeh Rezaie:** Conceptualization, Methodology, Writing - review & editing. **John P. Tiefenbacher:** Writing - review & editing. **Saro Lee:** Writing - review & editing. **Huiyuan Bian:** Writing - review & editing.

#### Declaration of Competing Interest

The authors declare that they have no known competing financial interests or personal relationships that could have appeared to influence the work reported in this paper.

#### Acknowledgments

This research was supported by the Basic Research Project of the Korea Institute of Geoscience and Mineral Resources (KIGAM) and Project of Environmental Business Big Data Platform and Center Construction funded by the Ministry of Science and ICT. Also, we greatly appreciate the assistance of the editor, Prof. Emmanouil Anagnostou, and three anonymous reviewers for their constructive comments who helped improve the paper.

#### References

- Hossain Anni, A., Cohen, S., Praskiewicz, S., 2020. Sensitivity of urban flood simulations to stormwater infrastructure and soil infiltration. *J. Hydrol.* 588, 125028. <https://doi.org/10.1016/j.jhydrol.2020.125028>.
- Beckers, A., Dewals, B., Erpicum, S., Dujardin, S., Detrembleur, S., Teller, J., Piroton, M., Archambeau, P., 2013. Contribution of land use changes to future flood damage along the river Meuse in the Wallon region. *Nat. Hazards Earth Syst. Sci.* <https://doi.org/10.5194/nhess-13-2301-2013>.
- Bengio, Y., Simard, P., Frasconi, P., 1994. Learning long-term dependencies with gradient descent is difficult. *IEEE Trans. Neural Networks* 5 (2), 157–166.
- Beven, K.J., Kirkby, M.J., 1979. A physically based, variable contributing area model of basin hydrology. *Hydrolog. Sci. Bull.* 24, 43–69. <https://doi.org/10.1080/0262667909491834>.
- Burrough, P.A., McDonnell, R.A., 1998. *Principles of geographical information systems*. Oxford University Press, Oxford, New York.
- Büchele, B., Kreibich, H., Kron, A., Thieken, A., Ihringer, J., Oberle, P., Merz, B., Nestmann, F., 2006. Flood-risk mapping: contributions towards an enhanced assessment of extreme events and associated risks. *Nat. Hazards Earth Syst. Sci.* 6 (4), 485–503.
- Chang, F.-J., Chen, P.-A., Lu, Y.-R., Huang, E., Chang, K.-Y., 2014. Real-time multi-step-ahead water level forecasting by recurrent neural networks for urban flood control. *J. Hydrol.* 517, 836–846.
- Cherqui, F., Belmeziti, A., Granger, D., Sourdril, A., Le Gauffre, P., 2015. Assessing urban potential flooding risk and identifying effective risk-reduction measures. *Sci. Total Environ.* 514, 418–425.
- Darabi, H., Choubin, B., Rahmati, O., Torabi Haghghi, A., Pradhan, B., Kløve, B., 2019. Urban flood risk mapping using the GARP and QUEST models: A comparative study of machine learning techniques. *J. Hydrol.* 569, 142–154.
- Davis, J., Goadrich, M., 2006, June. The relationship between Precision-Recall and ROC curves. In Proceedings of the 23rd international conference on Machine learning (pp. 233–240).
- De Reu, J., Bourgeois, J., Bats, M., Zwertiaegher, A., Gelorini, V., De Smedt, P., Chu, W., Antrop, M., De Maeyer, P., Finke, P., Van Meirvenne, M., Verniers, J., Crombé, P., 2013. Application of the topographic position index to heterogeneous landscapes. *Geomorphology* 186, 39–49. <https://doi.org/10.1016/j.geomorph.2012.12.015>.
- Easterling, D.R., Evans, J.L., Groisman, P.Y., Karl, T.R., Kunkel, K.E., Ambenje, P., 2000. Observed variability and trends in extreme climate events: a brief review. *Bull. Am. Meteorol. Soc.* 81 (3), 417–425.
- Eini, M., Kaboli, H.S., Rashidian, M., Hedayat, H., 2020. Hazard and vulnerability in urban flood risk mapping: Machine learning techniques and considering the role of urban districts. *Int. J. Disaster Risk Reduct.* 0–0 <https://doi.org/10.1016/j.ijdrr.2020.101687>.
- Eum, J.H., 2008. *Integration of Climate Information into Spatial Planning in Seoul, South Korea*. PhD dissertation. Technical University of Berlin, Berlin.
- Falah, F., Rahmati, O., Rostami, M., Ahmadisharaf, E., Daliakopoulos, I.N., Pourghasemi, H.R., 2019. Artificial Neural Networks for Flood Susceptibility Mapping in Data-Scarce Urban Areas. In *Spatial Modeling in GIS and R for Earth and Environmental Sciences*; Elsevier: Amsterdam, The Netherlands 2019, 323–336.
- Fernández, D.S., Lutz, M.A., 2010. Urban flood hazard zoning in Tucumán Province, Argentina, using GIS and multicriteria decision analysis. *Eng. Geol.* 111 (1–4), 90–98.

- Ferreira, C.S.S., Walsh, R.P.D., Steenhuis, T.S., Ferreira, A.J.D., 2018. Effect of Peri-urban Development and Lithology on Streamflow in a Mediterranean Catchment. *Land Degrad. Dev.* 29, 1141–1153.
- Gajowniczek, K., Ząbkowski, T., Szupiluk R., 2014, Estimating the ROC curve and its significance for classification model assessment, QUANTITATIVE METHODS IN ECONOMICS Vol. XV, No. 2, 2014, pp. 382 – 391.
- Gigović, L., Pamučar, D., Bajić, Z., Drobniak, S., 2017. Application of GIS-interval rough AHP methodology for flood hazard mapping in urban areas. *Water* 9 (6), 360.
- Gopalakrishnan, K., Khaitan, S.K., Choudhary, A., Agrawal, A., 2017. Deep convolutional neural networks with transfer learning for computer vision-based data-driven pavement distress detection. *Constr. Build. Mater.* 157, 322–330.
- Graves, A., Mohamed, A., Hinton, G. 2013. Speech recognition with deep recurrent neural networks. In Acoustics, speech and signal processing (icassp), 2013 ieee international conference on, pages 6645–6649. IEEE, 2013.
- Guisan, A., Weiss, S.B., Weiss, A.D., 1999. GLM versus CCA spatial modeling of plant species distribution. *Plant Ecol.* <https://doi.org/10.1023/A:1009841519580>.
- Guo, Z., Leitão, J.P., Simões, N.E., Moosavi, V., 2021. Data-driven flood emulation: Speeding up urban flood predictions by deep convolutional neural networks. *J. Flood Risk Manage.* 14 (1) <https://doi.org/10.1111/jfr3.v14.110.1111/jfr3.12684>.
- Ha, K.J., Shin, S.H., Mahrt, L., 2009. Spatial variation of the regional wind field with land-sea contrasts and complex topography. *J Appl Meteorol Climatol* 48, 1929–1939.
- Hales, M., Pena, A.M., Peterson, E.R., Dessibourg, N. 2018, ‘2018 Global cities report’, AT Kearney. Available from: [www.atkearney.com/2018-global-cities-report](http://www.atkearney.com/2018-global-cities-report) [23 July 2018].
- Hammond, M.J., Chen, A.S., Djordjević, S., Butler, D., Mark, O., 2015. Urban flood impact assessment: A state-of-the-art review. *Urban Water J.* 12 (1), 14–29.
- Hong, H., Panahi, M., Shirzadi, A., Ma, T., Liu, J., Zhu, A.X., Chen, W., Kougias, I., Kazakis, N., 2018. Flood susceptibility assessment in Hengfeng area coupling adaptive neuro-fuzzy inference system with genetic algorithm and differential evolution. *Sci. Total Environ.* doi:10.1016/j.scitotenv.2017.10.114.
- Hu, F., Xia, G.S., Hu, J., Zhang, L., 2015. Transferring deep convolutional neural networks for the scene classification of high-resolution remote sensing imagery. *Remote Sensing* 7 (11), 14680–14707.
- Hussain, D., Hussain, T., Khan, A.A., Naqvi, S.A.A., Jamil, A., 2020. A deep learning approach for hydrological time-series prediction: A case study of Gilgit river basin. *Earth Sci. Inf.* 13 (3), 915–927.
- Kalantari, Z., Ferreira, C.S.S., Koutsouris, A.J., Ahlmer, A.-K., Cerdà, A., Destouni, G., 2019. Assessing Flood Probability for Transportation Infrastructure Based on Catchment Characteristics, Sediment Connectivity and Remotely Sensed Soil Moisture. *Sci. Total Environ.* 661, 393–406.
- Kalantari, Z., Ferreira, C.S.S., Walsh, R.P.D., Ferreira, A.J.D., Destouni, G., 2017. Urbanization development under climate change: hydrological responses in a peri-urban Mediterranean catchment. *Land Degrad. Dev.* 28 (7), 2207–2221.
- Kang, X., Song, B., Sun, F., 2019. A deep similarity metric method based on incomplete data for traffic anomaly detection in IoT. *Appl. Sci.* 9 (1), 135. <https://doi.org/10.3390/app9010135>.
- Karamouz, M., Hosseinpour, A., Nazif, S., 2011. Improvement of urban drainage system performance under climate change impact: case study. *J. Hydrol. Eng.* 16 (5), 395–412.
- Karimi, S., Shiri, J., Kisi, O., Xu, T., 2018. Forecasting daily streamflow values: Assessing heuristic models. *Hydrolog. Res.* 49 (3), 658–669.
- Kato, T., Endo, A., 2017. Contrasting Two Dimensions of Disaster-Induced Water-Shortage Experiences: Water Availability and Access. *Water* 2017 (9), 982.
- Khan, A., Sohail, A., Zahroo, U., Qureshi, A.S., 2020. A survey of the recent architectures of deep convolutional neural networks. *Artif. Intell. Rev.* <https://doi.org/10.1007/s10462-020-09825-6>. Springer Nature B.V. 2020.
- Khosravi, K., Pham, B.T., Chapi, K., Shirzadi, A., Shahabi, H., Revhaug, I., Prakash, I., Tien Bui, D., 2018. A comparative assessment of decision trees algorithms for flash flood susceptibility modeling at Haraz watershed, northern Iran. *Sci. Total Environ.* doi:10.1016/j.scitotenv.2018.01.266.
- Kim, H.M., Han, S.S., 2012. Seoul. Cities, 29(2), 142–154.
- Kim, H.S., Chung, Y.S., Tans, P.P., Yoon, M.B., 2016. Climatological variability of air temperature and precipitation observed in South Korea for the last 50 years. *Air Qual. Atmos. Health* 2016 (9), 645–651.
- Kimura, N., Yoshinaga, I., Sekijima, K., Azechi, I., Baba, D., 2020. Convolutional neural network coupled with a transfer-learning approach for time-series flood predictions. *Water* 12 (1), 96.
- Kourgialas, N.N., Karatzas, G.P., 2011. Flood management and a GIS modeling method to assess flood-hazard areas—a case study. *Hydrol. Sci. J.* 56, 212–225.
- Kumar, P., Hati, A.S., 2020. Deep convolutional neural network based on adaptive gradient optimizer for fault detection in SCIM. *ISA Trans.* 111, 350–359.
- Lee, S., Lee, S., Lee, M.-J., Jung, H.-S., 2018. Spatial assessment of urban flood susceptibility using data mining and Geographic Information System (GIS) Tools. *Sustainability* 10 (3), 648. <https://doi.org/10.3390/su10030648>.
- Lee, S., Kim, J.-C., Jung, H.-S., Lee, M.J., Lee, S., 2017. Spatial prediction of flood susceptibility using random-forest and boosted tree models in Seoul metropolitan city. *Korea. Geomatics, Natural Hazards and Risk.* 8 (2), 1185–1203. <https://doi.org/10.1080/19475705.2017.1308971>.
- Li, K., Wu, S., Dai, E., Xu, Z., 2012. Flood loss analysis and quantitative risk assessment in China. *Nat. Hazards.* doi:10.1007/s11069-012-0180-y.
- Li, Y.u., Martinis, S., Wieland, M., 2019. Urban flood mapping with an active self-learning convolutional neural network based on TerraSAR-X intensity and interferometric coherence. *ISPRS J. Photogramm. Remote Sens.* 152, 178–191.
- Mao, J., Xu, W., Yang, Y., Wang, J., Huang, Z., Yuille, A. 2014. Deep captioning with multimodal recurrent neural networks (m-rnn). *arXiv preprint arXiv:1412.6632*, 2014.
- Meyer, H., Reudenbach, C., Wöllauer, S., Nauss, T., 2019. Importance of spatial predictor variable selection in machine learning applications—Moving from data reproduction to spatial prediction. *Ecol. Model.* 411, 108815. <https://doi.org/10.1016/j.ecolmodel.2019.108815>.
- Michelsen, A., Kalantari, Z., Lyon, S.W., Liljegren, E., 2016. Predicting and communicating flood risk of transport infrastructure based on watershed characteristics. *J. Environ. Manage.* 182, 505–518. <https://doi.org/10.1016/j.jenvman.2016.07.051>.
- Mignot, E., Li, X., Dewals, B., 2019. Experimental modelling of urban flooding: A review. *J. Hydrol.* 568, 334–342.
- Mikolov, T., Joulin, A., Chopra, S., Mathieu, M., Ranzato, M. 2006. “Learning longer memory in recurrent neural networks,” *arXiv preprint arXiv:1412.7753*, 2014.
- Mokarrama, M., Hojati, M., 2018. Landform classification using a sub-pixel spatial attraction model to increase spatial resolution of digital elevation model (DEM). *Egypt. J. Remote Sens. Sp. Sci.* doi:10.1016/j.ejrs.2016.11.005.
- Moore, I.D., Grayson, R.B., Ladson, A.R., 1991. Digital terrain modelling: A review of hydrological, geomorphological, and biological applications. *Hydrolog. Process.* doi: 10.1002/hyp.3360050103.
- Naito, A.T., Cairns, D.M., 2011. Relationships between Arctic shrub dynamics and topographically derived hydrologic characteristics. *Environ. Res. Lett.* doi:10.1088/1748-9326/6/4/045506.
- Nguyen, D.H., Bae, D.-H., 2020. Correcting mean areal precipitation forecasts to improve urban flooding predictions by using long short-term memory network. *J. Hydrol.* 584, 124710. <https://doi.org/10.1016/j.jhydrol.2020.124710>.
- Nourani, V., Hosseini Baghanam, A., Adamowski, J., Kisi, O., 2014. Applications of hybrid wavelet-artificial intelligence models in hydrology: a review. *J. Hydrol.* 514, 358–377.
- Park, M.H., Ju, M., Cho, Y.H., Kim, J.Y., 2020. Data stratification toward advanced flood waste estimation: A case study in South Korea. *Waste Manage.* 114, 215–224.
- Peng, B., Meng, Z., Huang, Q., Wang, C., 2019. Patch similarity convolutional neural network for urban flood extent mapping using bi-temporal satellite multispectral imagery. *Remote Sensing* 11 (21), 2492.
- Petneházi, G., 2019. Recurrent neural networks for time series forecasting. *arXiv preprint arXiv:1901.00069*.
- Petty, T.R., Dhingra, P., 2018. Streamflow hydrology estimate using machine learning (SHEM). *JAWRA J. Am. Water Resources Association* 54 (1), 55–68.
- Popa, M.C., Peptenatu, D., Draghici, C.C., Diaconu, D.C., 2019. Flood hazard mapping using the flood and Flash-Flood Potential Index in the Buzau River catchment. *Romania. Water* (Switzerland). <https://doi.org/10.3390/w11102116>.
- Predick, K.I., Turner, M.G., 2008. Landscape configuration and flood frequency influence invasive shrubs in floodplain forests of the Wisconsin River (USA). *J. Ecol.* doi: 10.1111/j.1365-2745.2007.01329.x.
- Radula, M.W., Szymura, T.H., Szymura, M., 2018. Topographic wetness index explains soil moisture better than bioindication with Ellenberg’s indicator values. *Ecol. Indic.* doi:10.1016/j.ecolind.2017.10.011.
- Rahmati, O., Darabi, H., Haghghi, A.T., Stefanidis, S., Kornejady, A., Nalivan, O.A., Tien Bui, D., 2019. Urban Flood Hazard Modeling Using Self-Organizing Map Neural Network. *Water* 11 (11), 2370.
- Rahmati, O., Darabi, H., Panahi, M., Kalantari, Z., Naghibi, S.A., Ferreira, C.S.S., Kornejady, A., Karimadestanei, Z., Mohammadi, F., Stefanidis, S., Bui, D.T., Haghghi, A.T., 2020. Development of novel hybridized models for urban flood susceptibility mapping. *Sci. Rep.* 10, 12937.
- Rejith, R.G., Anirudhan, S., Sundararajan, M., 2019. Delineation of groundwater potential zones in hard rock terrain using integrated remote sensing, GIS and MCDM techniques: A case study from vamanapuram river basin, Kerala, India, in: *GIS and Geostatistical Techniques for Groundwater Science*. doi:10.1016/B978-0-12-815413-7.00025-0.
- Ren, T., Liu, X., Niu, J., Lei, X., Zhang, Z., 2020. Real-time water level prediction of cascaded channels based on multilayer perception and recurrent neural network. *J. Hydrol.* 585, 124783. <https://doi.org/10.1016/j.jhydrol.2020.124783>.
- Righini, M., Surian, N., Wohl, E., Marchi, L., Comiti, F., Ampsonah, W., Borga, M., 2017. Geomorphic response to an extreme flood in two Mediterranean rivers (northeastern Sardinia, Italy): Analysis of controlling factors. *Geomorphology*. doi:10.1016/j.geomorph.2017.04.014.
- Riley, S.J., DeGloria, S.D., Elliot, R., 1999. A terrain ruggedness index that quantifies topographic heterogeneity. *Intermt. J. Sci.* 5, 23–27.
- Rodríguez, J.L.G., Suárez, M.C.G., 2010. Estimation of slope length value of RUSLE factor L using GIS. *J. Hydrol. Eng.* 15 (9), 714–717.
- Sanders, B.F. 2007. Evaluation of on-line DEMs for flood inundation modeling. *Advances in Water Resources*, v. 30, n. 8, p. 1831–1843, Ago. 2007.
- Sato, T., 2006. Fundamental characteristics of flood risk in Japan’s urban areas. *Better Integrated Management of Disaster Risks: Toward Resilient Society to Emerging Disaster Risks in Mega-cities*. Terra Scientific Publishing Company: Tokyo, pp.23–40.
- Sepehri, M., Malekinezhad, H., Hosseini, S.Z., Ildoromi, A.R., 2019. Assessment of flood hazard mapping in urban areas using entropy weighting method: a case study in Hamadan city. *Iran. Acta Geophysica* 67 (5), 1435–1449.
- Shin, S., Park, C., 2014. Analyzing Relationships between Land Use Characteristics and Flood Damage Areas: The Case of Seoul. *Korea Spat. Plan. Rev.* 2014 (81), 3–20.
- Shiri, J., Kisi, O., 2010. Short-term and long-term streamflow forecasting using a wavelet and neuro-fuzzy conjunction model. *J. Hydrol.* 394 (3-4), 486–493.
- Shiri, J., Kiş, Ö., Makarynsky, O., Shiri, A.-A., Nikoofar, B., 2012. Forecasting daily stream flows using artificial intelligence approaches. *ISH Journal of Hydraulic Engineering* 18 (3), 204–214.

- Socher, R., Lin, C., Manning, C., Y Ng. A. 2011. Parsing natural scenes and natural language with recursive neural networks. In Proceedings of the 28th international conference on machine learning (ICML-11), pages 129–136, 2011.
- Sutskever, I., Martens, J., Hinton, G.E. 2011. “Generating text with recurrent neural networks,” in Proceedings of the 28th International Conference on Machine Learning (ICML-11), 2011, pp. 1017–1024.
- Sutskever, I., Martens, J., Dahl, G., Hinton, G., 2013. February. On the importance of initialization and momentum in deep learning. In: In International conference on machine learning, pp. 1139–1147.
- Tehrany, M.S., Pradhan, B., Jebur, M.N., 2014. Flood susceptibility mapping using a novel ensemble weights-of-evidence and support vector machine models in GIS. *J Hydrol.* 512, 332–343.
- Tehrany, M.S., Pradhan, B., Mansor, S., Ahmad, N., 2015a. Flood susceptibility assessment using GIS-based support vector machine model with different kernel types. *Catena* 125, 91–101.
- Tehrany, M.S., Pradhan, B., Jebur, M.N., 2015b. Flood susceptibility analysis and its verification using a novel ensemble support vector machine and frequency ratio method. *Stoch. Env. Res. Risk A.* 29 (4), 1149–1165.
- Teng, J., Jakeman, A.J., Vaze, J., Croke, B.F.W., Dutta, D., Kim, S., 2017. Flood inundation modelling: A review of methods, recent advances and uncertainty analysis. *Environ. Modell. Software* 90, 201–216.
- Tockner, K., Lorang, M.S., Stanford, J.A., 2010. River flood plains are model ecosystems to test general hydrogeomorphic and ecological concepts. *River Res. Appl.* 26 (1), 76–86.
- UN-Water, 2020. United Nations World Water Development Report 2020: Water and Climate Change, Paris, UNESCO.
- Wang, Y., Hong, H., Chen, W., Li, S., Panahi, M., Khosravi, K., Shirzadi, A., Shahabi, H., Panahi, S., Costache, R., 2019. Flood susceptibility mapping in Dingnan County (China) using adaptive neuro-fuzzy inference system with biogeography based optimization and imperialistic competitive algorithm. *J. Environ. Manage.* 247, 712–729.
- Weiss, A., 2001. Topographic position and landforms analysis, in: ESRI User Conference, San Diego, USA.
- Williamson, B.D., Gilbert, P.B., Carone, M., Simon, N., 2021. Nonparametric variable importance assessment using machine learning techniques. *Biometrics* 77 (1), 9–22.
- Wilson, J.P., Gallant, J.C., 2000. Secondary topographic attributes, in: J.P., W., J.C., G. (Eds.), *Terrain Analysis: Principles and Applications*. Wiley, Toronto, Canada, p. 479.
- Wu, J. 2020. Convolutional neural networks, LAMDA GroupNational Key Lab for Novel Software Technology Nanjing University.
- Wu, S., Flach, P., 2005. August. A scored AUC metric for classifier evaluation and selection. In Second Workshop on ROC Analysis in ML, Bonn, Germany.
- Xia, J., Du, X., Xu, W., Wei, Y., Xiong, Y., Min, S., 2021. Non-destructive analysis the dating of paper based on convolutional neural network. *Spectrochim. Acta Part A Mol. Biomol. Spectrosc.* 248, 119290. <https://doi.org/10.1016/j.saa.2020.119290>.
- Xu, H., Ma, C., Lian, J., Xu, K., Chaima, E., 2018. Urban flooding risk assessment based on an integrated k-means cluster algorithm and improved entropy weight method in the region of Haikou, China. *J. Hydrol.* 563, 975–986.
- Xu, H., Mannor, S., 2012. Robustness and generalization. *Machine Learning* 86 (3), 391–423.
- Yesilnacar, E.K. 2005. The application of computational intelligence to landslide susceptibility mapping in Turkey. Ph.D Thesis Department of Geomatics the University of Melbourne 423 pp.
- Zhang, S., Pan, B., 2014. An urban storm-inundation simulation method based on GIS. *J. Hydrol.* 517, 260–268.
- Zhao, G., Pang, B., Xu, Z., Peng, D., Zuo, D., 2020. Urban flood susceptibility assessment based on convolutional neural networks. *J. Hydrol.* 590, 125235. <https://doi.org/10.1016/j.jhydrol.2020.125235>.
- Zhao, G., Xu, Z., Pang, B., Tu, T., Xu, L., Du, L., 2019. An enhanced inundation method for urban flood hazard mapping at the large catchment scale. *J. Hydrol.* 571, 873–882.